communications physics

ARTICLE

https://doi.org/10.1038/s42005-023-01289-8 OPEN

Unusual crossover from Bardeen-Cooper-Schrieffer to Bose-Einstein-condensate superconductivity in iron chalcogenides

Yuta Mizukami[1,2✉], Masahiro Haze[3,4], Ohei Tanaka[1], Kohei Matsuura[1,5], Daiki Sano[3], Jakob Böker[6], Ilya Eremin[6], Shigeru Kasahara[3,7], Yuji Matsuda[3] & Takasada Shibauchi[1]

The BCS-BEC (Bardeen-Cooper-Schrieffer–Bose-Einstein-condensate) crossover from strongly overlapping Cooper pairs to non-overlapping composite bosons in the strong coupling limit has been a long-standing issue of interacting many-body fermion systems. Recently, FeSe semimetal with hole and electron bands emerged as a high-transition-temperature (high-T_c) superconductor located in the BCS-BEC crossover regime, owing to its very small Fermi energies. In FeSe, however, an ordinary BCS-like heat-capacity jump is observed at T_c, posing a fundamental question on the characteristics of the BCS-BEC crossover. Here we report on high-resolution heat capacity, magnetic torque, and scanning tunneling spectroscopy measurements in $FeSe_{1-x}S_x$. Upon entering the tetragonal phase at $x > 0.17$, where nematic order is suppressed, T_c discontinuously decreases. In this phase, highly non-mean-field behaviours consistent with BEC-like pairing are found in the thermodynamic quantities with giant superconducting fluctuations extending far above T_c, implying the change of pairing nature. Moreover, the pseudogap formation, which is expected in BCS-BEC crossover of single-band superconductors, is not observed in the tunneling spectra. These results illuminate highly unusual features of the superconducting states in the crossover regime with multiband electronic structure and competing electronic instabilities.

[1] Department of Advanced Materials Science, University of Tokyo, Chiba 277-8561, Japan. [2] Department of Physics, Tohoku University, 6-3, Aramaki Aza-Aoba, Aoba-Ku, Sendai 980-8578, Japan. [3] Department of Physics, Kyoto University, Sakyo-ku, Kyoto 606-8502, Japan. [4] Institute for Solid State Physics, University of Tokyo, Kashiwa, Chiba 277-8581, Japan. [5] Department of Applied Physics, University of Tokyo, Hongo, Bunkyo-Ku Tokyo 113-8656, Japan. [6] Institut fur Theoretische Physik III, Ruhr-Universitat Bochum, D-44801 Bochum, Germany. [7] Research Institute for Interdisciplinary Science, Okayama University, Okayama 700-8530, Japan. ✉email: mizukami@tohoku.ac.jp

The crossover between the weak-coupling Bardeen–Cooper–Schrieffer (BCS) theory of superconductivity and strong-coupling Bose–Einstein-condensate (BEC) describes the fundamentals of quantum bound states of particles, including information on the superconducting critical temperature (T_c) and the possible pseudogap formation[1–3]. In the strong-coupling regime, the pair-formation temperature T_{pair} and the actual superconducting transition temperature T_c are distinctly separated (Fig. 1a). Between T_{pair} and T_c, the so-called preformed Cooper pairs exist, which give rise to large superconducting fluctuations and possibly a depletion of the low-energy density of states (DOS), namely the pseudogap. Almost all experimental studies on crossover physics have been performed in ultracold atomic systems for the past decades[2] because of the difficulty in tuning the attractive interaction between electrons in solids. Therefore, it is extremely challenging to realize such strongly coupled pairs in electron systems. In underdoped high-T_c cuprates, the pseudogap formation has been discussed in terms of the BCS–BEC crossover[4], but recent experiments support a phase transition of different kinds at the onset of the pseudogap, and the relevance of BCS–BEC crossover in cuprates remains unresolved[5]. On the other hand, very recent studies have successively pointed to the realization of BCS–BEC crossover in superconductivity in other strongly correlated compounds[6–9].

The superconducting semimetal FeSe[10–12] with very small hole and electron Fermi surfaces are found to exhibit large ratios of the superconducting energy gap Δ and Fermi energy E_F, $\Delta/E_F \approx 0.3$–1.0[7,13,14], which appears to place FeSe in the crossover regime (Fig. 1a). Indeed, in high-quality single crystals with long mean free paths of electrons[7], large superconducting fluctuations have been reported from the torque magnetometry, providing support for the presence of fluctuated Cooper pairs created above T_c in the crossover regime[15]. These observations underline the importance of the BCS-BEC crossover physics both in the superconducting and normal states of FeSe. On the other hand, scanning tunneling spectroscopy (STS) measurements do not observe the pseudogap formation above T_c[16].

These results imply that the superconductivity in FeSe is not simply described by a picture of the conventional BCS-BEC crossover. An important aspect that has not been taken into account in the previous studies is the effects of multiband electronic structure, which may have other tuning factors of the crossover in addition to Δ/E_F. In fact, the Fermi surface of FeSe is composed of separated holes and electron pockets with different values of Δ/E_F[7,13,17]. It has been pointed out that in multiband systems, the developments of superconducting fluctuations and pseudogap formation are sensitively affected by the interband coupling strength[18–20], indicating that the normal and superconducting properties associated with the crossover in multiband systems can be different from those in the single band systems[21]. It is quite important, therefore, to clarify how the superconducting properties evolve when the multiband electronic structure is tuned.

Here, we focus on $FeSe_{1-x}S_x$, where the orthorhombic (nematic) phase transition at 90 K in FeSe can be tuned by isovalent sulfur (S) substitution. The nematic transition that distorts the Fermi surface is completely suppressed at a critical concentration $x_c \approx 0.17$[22,23]. The superconductivity persists in the tetragonal (non-nematic) phase above x_c. In the case of applying hydrostatic pressure, the suppression of nematic order is accompanied by the pressure-induced antiferromagnetic order[24]. In contrast, S substitution suppresses the nematic order without inducing the antiferromagnetism that significantly changes the Fermi surface through band folding, even when crossing x_c. This enables us to investigate the evolution of the superconducting state in the BCS–BEC crossover with little influence of antiferromagnetic fluctuations. Moreover, the observations of

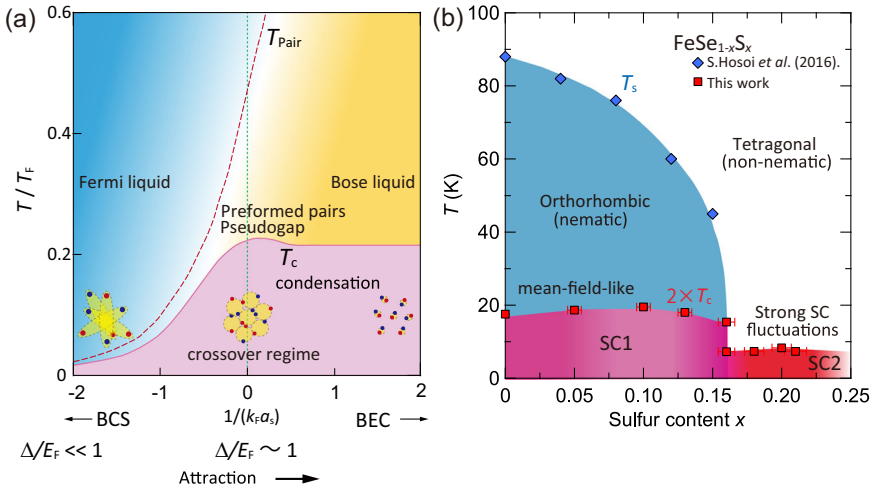

Fig. 1 Phase diagrams of BCS-BEC (Bardeen-Cooper-Schrieffer-Bose-Einstein-condensate) crossover in single-band systems and multiband $FeSe_{1-x}S_x$ superconductors. a Theoretical phase diagram of BCS-BEC crossover generally obtained for single-band systems[1,2]. The temperature T is normalized by the Fermi temperature T_F, and the strength of attraction is given by dimensionless coupling constant $1/(k_Fa_s)$. Here, k_F and a_s are Fermi wavenumber and *s*-wave-scattering length, respectively. Below the pairing temperature T_{pair}, bosonic pairs form, while the superconducting coherence is acquired when the condensation occurs at superconducting transition temperature T_c. In the weak-coupling BCS limit, the ratio of the superconducting gap and Fermi energy Δ/E_F is much smaller than unity, and the coherence length ξ is much longer than the interparticle distance (~$1/k_F$), and T_{pair} is very close to the actual T_c. In the BCS–BEC crossover regime Δ/E_F ~1, T_c/T_F reaches a maximum, and preformed Cooper pairs are expected to exist in an extended temperature region between T_{pair} and T_c. **b** Experimentally determined T–x phase diagram of $FeSe_{1-x}S_x$. The superconducting transition temperature T_c (red squares) is determined by the present heat capacity measurements using small crystals. The nematic transition temperature (blue diamonds) determined by transport measurements[22] is also plotted. The abrupt change in T_c indicates a significantly different superconducting ground state between SC (superconducting state)1 and SC2 divided by the nematic end point at $x_c \approx 0.17$. The error bars are determined by the distribution of the chemical composition in the samples.

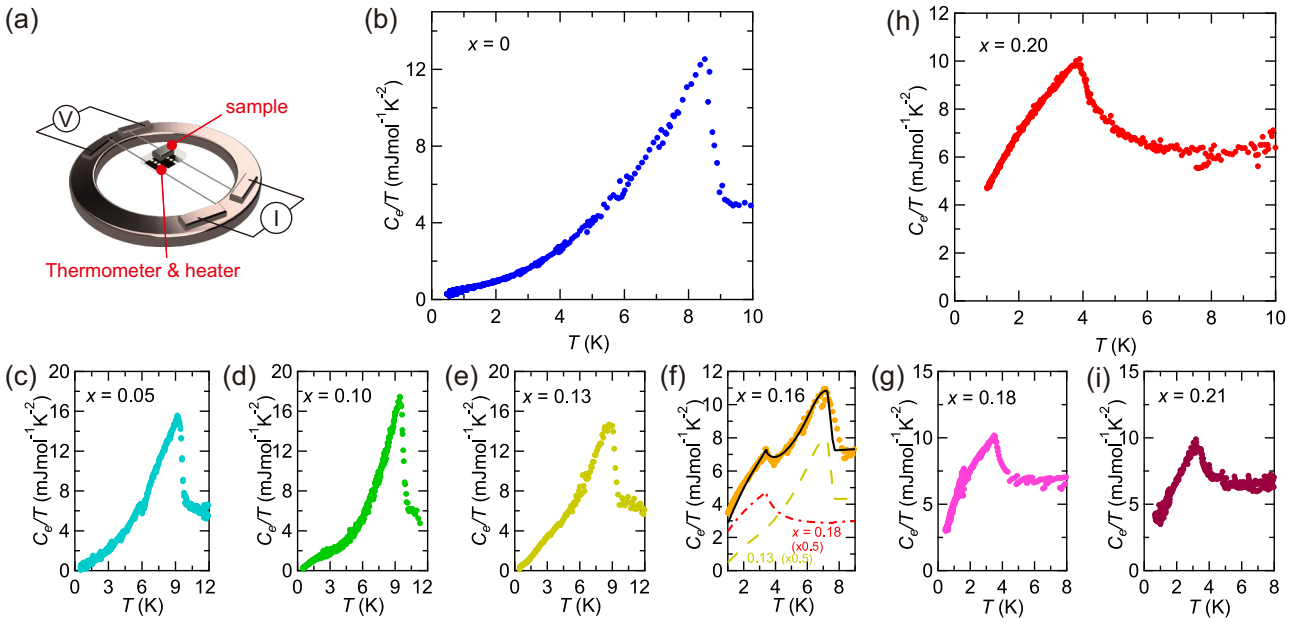

Fig. 2 Heat capacity in $FeSe_{1-x}S_x$ superconductors. a The schematic of the experimental setup. A Cernox small thermometer chip is used as a heater, and large current pulses are applied. **b–i** *T*-dependence of electronic heat capacity divided by *T*, C_e/T in $FeSe_{1-x}S_x$ single crystals at low temperatures for $x = 0$ (**b**), $x = 0.05$ (**c**), $x = 0.10$ (**d**), $x = 0.13$ (**e**) in the orthorhombic phase and $x = 0.18$ (**g**), $x = 0.20$ (**h**), $x = 0.21$ (**i**) in the tetragonal phase. **f** *T*-dependence of C_e/T for $x = 0.16$ near the nematic end point. The data (orange dots) are fitted with a weighted sum (black line) of the $x = 0.13$ orthorhombic data (dashed line) and $x = 0.18$ tetragonal data (dashed-dotted line) with adjusted T_c values.

quantum oscillations up to $x \approx 0.19$[25] demonstrate that the S ions do not act as strong scattering centers.

By using high-resolution heat capacity, magnetic torque, and scanning tunneling spectroscopy measurements, we clarify the unusual evolution of the thermodynamic and spectroscopic properties in the $FeSe_{1-x}S_x$ system, where the highly non-mean-field behaviors are found in tetragonal phase $x > 0.17$ with no signature of pseudogap formation. These results illuminate the unusual feature of BCS–BEC crossover with the multiband electronic structure.

Results and Discussion

Heat capacity. Through the high-resolution heat capacity, magnetic torque, and STS measurements on high-quality single crystals, we investigate the evolution of superconducting and normal state properties with *x* in $FeSe_{1-x}S_x$. In Fig. 1b, we show the phase diagram obtained by the heat capacity measurements. The drastic change in T_c and superconducting fluctuations are found across x_c. To ensure sample homogeneity, we used very small crystals (10–190 μg) for the thermodynamic measurements and employed the long relaxation method with a homemade cell (Fig. 2a) designed for small single crystals. Figure 2b–e depicts the *T*-dependence of electronic heat capacity divided by *T*, C_e/T, for $x = 0$, 0.05, 0.10, and 0.13. Here we subtract the phonon contribution, which shows T^3-dependence, as confirmed by the measurements in the normal state at high fields. In Fig. 2b, $C_e/T(T)$ in FeSe ($x = 0$) exhibits an ordinary BCS-like jump at $T_c = 9$ K, consistent with the previous studies on larger samples[26–28]. As the temperature is lowered below T_c, C_e/T decreases with decreasing slope. Below ~3 K, C_e/T shows *T*-linear dependence, which is consistent with the strongly anisotropic superconducting gap[7,28,29]. Similar $C_e/T(T)$ is observed in orthorhombic phase $x = 0.05$, 0.10, and 0.13 with T_c of 9.7, 10, and 9.5 K, respectively (Fig. 2c–e).

Upon entering the tetragonal phase at $x > x_c$, C_e/T exhibits a dramatic change not only in the superconducting state but also in the normal state. As represented by $x = 0.20$ in Fig. 2h, C_e/T increases with the increasing slope in the normal state when approaching T_c from high temperatures. In addition, C_e/T exhibits a kink at T_c without showing a discontinuous jump. Such a continuous *T*-dependence at T_c is reminiscent of the BEC transition in the free Bose gas systems[30], although it is too simple to employ the free Bose gas model in our system. We note that a similar enhancement of C_e/T in the normal state is obtained in the calculations for the strongly interacting Fermi systems near the unitary limit in the BCS–BEC crossover regime[31]. As the temperature is lowered below T_c, $C_e/T(T)$ for $x = 0.20$ decreases with increasing slope, in stark contrast to $C_e/T(T)$ in the orthorhombic crystals, as shown in Fig. 2b–e. Below T_c, C_e/T decreases sublinearly to *T* with large residual C_e/T at the lowest temperatures, which is indicative of a large DOS at zero energy. The large residual DOS is consistent with the recent thermal conductivity and STS measurements[32,33]. Similar $C_e/T(T)$ is also observed for $x = 0.18$ and 0.21 in the tetragonal phase, as shown in Fig. 2g, i. These results, together with the sharp change in T_c across x_c, demonstrate that the superconducting properties in the tetragonal phase are drastically different from those in the orthorhombic phase. We note that a similar broadening of C/T at T_c has also been observed when nematicity is suppressed by pressure[34].

We stress that the observed peculiar $C_e/T(T)$ in the tetragonal phase does not stem from chemical inhomogeneity within the small sample for the following reasons. First, the topographic image in STM of $FeSe_{1-x}S_x$ crystals reveals no evidence for the segregation of S atoms, indicating an excellent homogeneity[33] (see also Fig. 3a, b). Second, the observation of the quantum oscillations of the crystals in the same batch[25] demonstrates a long mean free path of the carriers, ensuring the high quality of our crystals. Third, according to the elemental mapping of the energy dispersive X-ray spectroscopy (EDX) at different scales of distance (Supplementary Note 1), the typical spatial variation of the composition Δx is ~ 0.01, and there are no discernible segregations or large inhomogeneity of the chemical compositions which can explain our observation in $C_e/T(T)$. Fourth, we measured the heat capacity on two different crystals for $x = 0.20$ (Supplementary Note 2) and two other concentrations, $x = 0.18$

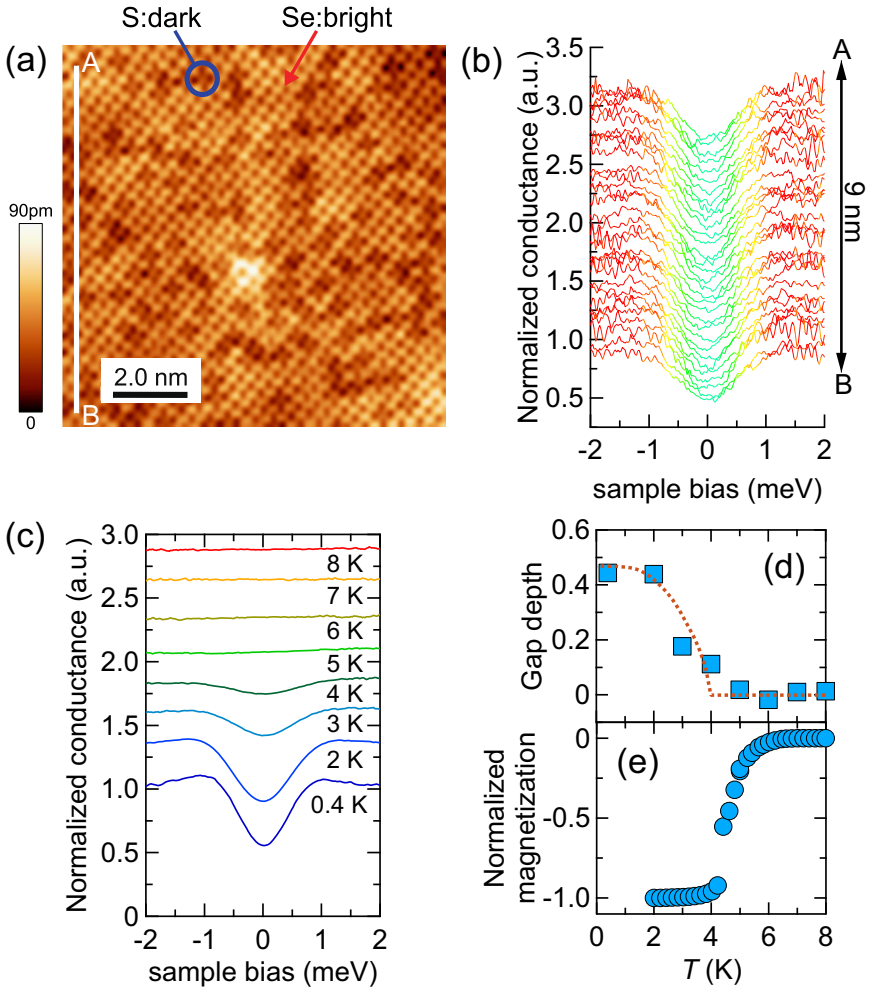

Fig. 3 Scanning tunneling spectroscopy in the tetragonal phase. a Topographic STM (scanning tunneling microscopy) image (10 mV, 100 pA) of $FeSe_{0.75}S_{0.25}$ surface over a 10 nm by 10 nm area. **b** A line profile of the normalized conductance along the AB is shown in (**a**). The data are taken at 2 K. **c** Normalized tunneling conductance spectra are taken at several temperatures. The spectra are vertically shifted for clarity. The tip is stabilized at bias voltage $V = 6$ mV and current $I = 1$ nA. **d** The T-dependence of gap depth, which is defined by the difference between normalized conductance values at $V = 0$ and 6 mV. The red dashed line is a guide for the eye. **e** The T-dependence of magnetization measured at a zero field cool condition.

and 0.21 (Fig. 2g, i), and confirmed the reproducibility of the behavior. We also note that our results are consistent with the previous data of the crystal with a much larger volume within the error bar (Supplementary Note 2). Fifth, most importantly, there is no concentration of the sample, which shows the superconducting transition between ≈ 4 K and ≈ 7 K in the phase diagram of $FeSe_{1-x}S_x$. This is supported by the $C_e/T(T)$ of the crystal at $x \approx 0.16$, which is located in the very vicinity of x_c. As shown in Fig. 2f, C_e/T at $x \approx 0.16$ exhibits two well-separated peaks at $T_{c1} = 4$ K and $T_{c2} = 7$ K, indicating a phase separation (due to the small spatial variation of $\Delta x \sim 0.01$) at x_c. This T-dependence is well reproduced by the sum of C_e/T of $x = 0.13$ ($T_c = 9.5$ K) and 0.18 ($T_c = 4.0$ K), assuming that both contribute equally. Here, for the fitting, T_c values are shifted slightly. These results indicate a discontinuous change of T_c at x_c. Such a discontinuous change in the superconducting properties is consistent with the jump in Δ values at x_c recently reported by STS studies[33]. The observed enhancement of C_e/T above T_c for the sample in the tetragonal phase, therefore, can be attributed to an intrinsic electronic property.

Scanning tunneling microscopy (STM)/spectroscopy (STS). To elucidate whether the depletion of DOS associated with the pseudogap formation occurs, the STS measurements on the crystal of $x = 0.25$ are performed. By counting the number of S atoms in the STM topographic image, we determined the x value accurately (Fig. 3a). Figure 3b shows the line profile of the normalized conductance along line AB depicted in Fig. 3a. Spectra show little variation within the 10 nm scale, demonstrating the uniform spatial distribution of the superconducting gap. We also note that the gap value is consistent with the previous report[33]. Figure 3c depicts the STS spectra normalized by the conductance above the superconducting gap in a wide temperature range. Large residual DOS, which is more than half of the normal state value outside the superconducting gap (Δ ≈ 1 meV), is observed even at $T = 0.4$ K ($T/T_c = 0.1$). This large residual DOS is consistent with the large C_e/T at low temperatures. Here, the STS spectrum becomes nearly energy independent at high temperatures above ~5 K, showing no signs of gap formation. This is also seen by the T-dependence of the gap depth plotted in Fig. 3d. The superconducting gap closes at ≈ 5 K, below which the T-dependence of magnetization shows a rapid decrease, as shown in Fig. 3e.

Nearly energy-independent DOS at E_F observed by STS above T_c indicates that the observed enhancement of C_e/T above T_c in the tetragonal phase is not caused by the DOS effect. Therefore, it is natural to consider that the enhancement of C_e/T stems from the superconducting fluctuations. Indeed, a similar enhancement

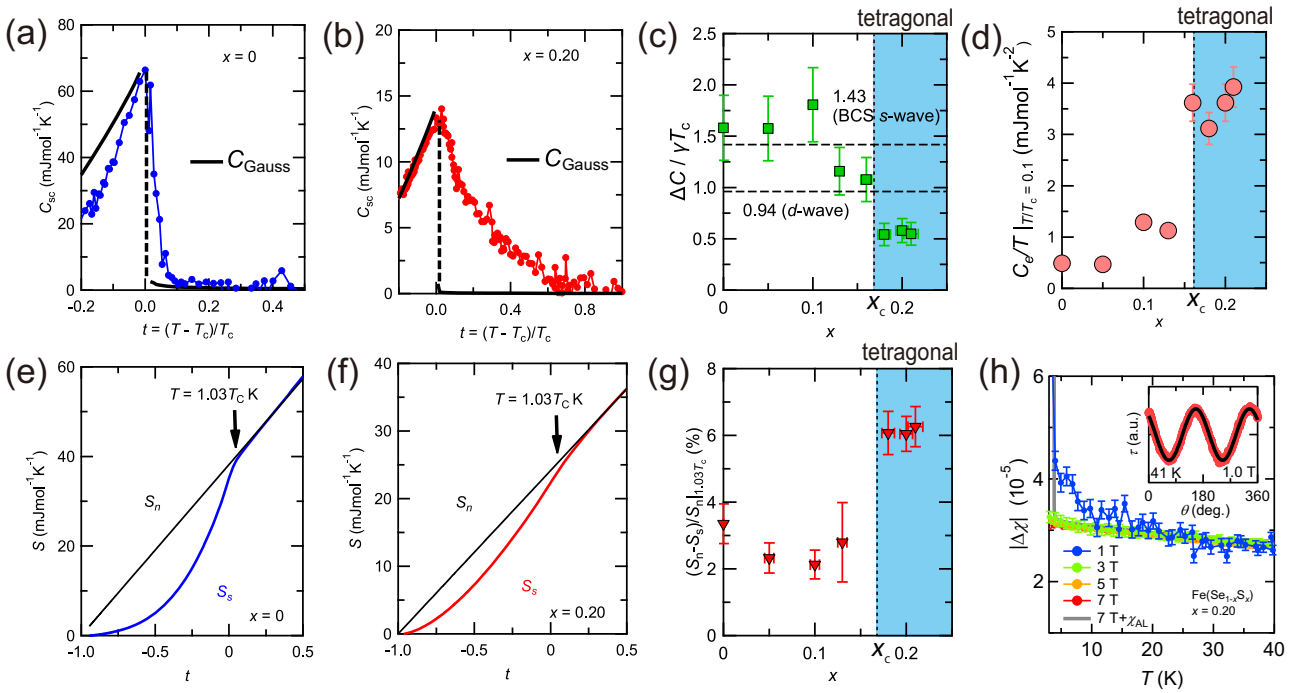

Fig. 4 Comparisons of superconducting transition properties between the orthorhombic and tetragonal phases. a, **b** The superconducting contribution to the electronic heat capacity $C_{sc} = C_e - \gamma T$ as a function of reduced temperature $t \equiv \frac{T-T_c}{T_c}$ for $x = 0$ (**a**) and $x = 0.20$ (**b**). The conventional Gaussian fluctuation contribution C_{Gauss} is estimated (solid lines). **c**, **d** x dependence of $\Delta C/\gamma T_c$ (**c**), and C_e/T at $T/T_c = 0.1$ (**d**). **e**, **f** Entropy calculated from $C_e/T(T)$ in the normal state (S_n) and superconducting state (S_s) as a function of t for $x = 0$ (**e**) and $x = 0.20$ (**f**). S_n is estimated from the high-field data where superconductivity is suppressed. The entropy for $x = 0.20$ is linearly extrapolated below 1.0 K. **g** x dependence of the relative entropy difference between zero and high fields $(S_n - S_s)/S_n$ at $T = 1.03T_c$. **h** The T-dependence of the anisotropy of the magnetic susceptibility $\Delta\chi = \chi_c - \chi_{ab}$ for several fields in $x = 0.20$. Each data is obtained by fitting the field-angle dependence of the torque $\tau(\theta)$. The inset shows the $\tau(\theta)$ at 1.0 T and 41 K as the typical signal of torque, where the red markers and the solid black line show the raw data and fitting curve, respectively. The error bars are determined by the errors in estimating the volume of the sample and the error in the fitting procedure.

of C_e/T toward T_c due to the strong fluctuations has been previously reported in other iron-based superconductors[35–37]. In order to discuss the effect of the superconducting fluctuations in $FeSe_{1-x}S_x$ quantitatively, we extract the superconducting contribution C_{sc}, which is obtained by subtracting the normal state electronic contribution γT from C_e for $x = 0$ (blue circles in Fig. 4a) and $x = 0.20$ (red circles in Fig. 4b). We compare C_{sc} with the conventional term of the mean-field Gaussian fluctuations[38] (Supplementary Note 3). Obviously, the heat capacity contribution that significantly exceeds C_{Gauss} can be seen for $x = 0.20$. This extra heat capacity is observable up to $t \sim 0.8$. In Fig. 4c, we display the x-dependence of $\Delta C/\gamma T_c$, where ΔC is the height of C_{sc} at T_c. For $x < x_c$, the magnitude of $\Delta C/\gamma T_c$ is close to the BCS weak coupling value (1.43 for s-wave and 0.94 for d-wave). On the other hand, $\Delta C/\gamma T_c$ for $x > x_c$ is reduced far below the mean-field BCS value. As a consequence of the unusual suppression of $\Delta C/\gamma T_c$, the low-T C_e/T is largely enhanced through the entropy balance. Figure 4d depicts the x-dependence of the C_e/T at $T/T_c = 0.1$ taken from Fig. 2. Remarkable enhancement of C_e/T at x_c indicates the fundamental difference of the low-energy excitations across x_c. We note that recent NMR measurements for $x > x_c$ report no splitting of the spin-echo signal in the crystal from the same batch[39,40], which excludes the microscopic phase separation of superconducting and non-superconducting regions.

Magnetic torque. The anomalous C_e/T in the tetragonal phase is reflected by the entropies in the normal and superconducting states, S_n and S_s, respectively, as shown in Fig. 4e, f. For $x = 0$, the T-dependence of S_s shows a kink at T_c, which is typical for the second-order superconducting transition. For $x = 0.20$, on the other hand, owing to the absence of the jump in C_e/T at T_c, no kink anomaly is observed in the T-dependence of S_s. Moreover, the entropy is significantly suppressed from S_n even above T_c. In Fig. 4g, we show the x dependence of the lost entropy normalized by S_n, $(S_n - S_s)/S_n$, just above T_c, $T = 1.03T_c$. Upon entering the tetragonal phase, an abrupt enhancement of $(S_n - S_s)/S_n$ can be seen, indicating a drastic change of the superconducting fluctuations associated with the preformed Cooper pairs.

To obtain further insight into the superconducting fluctuations in the tetragonal phase, the magnetic torque was measured by using micro-cantilevers. The torque can sensitively detect the diamagnetic response through the anisotropy of magnetic susceptibility[15]. By measuring the field angular variation of torque as a function of polar angle θ from the c axis, the anisotropy $\Delta\chi = \chi_c - \chi_{ab}$ is determined, where χ_c and χ_{ab} are the magnetic susceptibilities along the c axis and in the ab plane, respectively. As shown in the inset of Fig. 4h, $\tau(\theta)$ shows an almost perfect sinusoidal curve, $\tau(\theta) \propto \Delta\chi \sin\theta$. Although $\Delta\chi(T)$ at high fields is almost independent of T and H, it exhibits strong T and H-dependence at low fields, as shown in Fig. 4h. It is well settled that the fluctuation-induced diamagnetic susceptibility of most superconductors, including multiband systems, can be well described by the standard Gaussian-type (Aslamasoz–Larkin, AL) fluctuation susceptibility χ_{AL} (Supplementary Note 3). Here we focus on the H-dependent diamagnetic susceptibility at low fields[15]. Then, $\Delta\chi$ at low fields is much larger than the $|\chi_{AL}|$, which is added to high field 7 T data. This implies that the superconducting fluctuations in $FeSe_{1-x}S_x$ are distinctly different from those in conventional superconductors, supporting the

fluctuation effects observed in heat capacity measurements. We stress that although the multi-gap superconductivity may lead to a small value of $\Delta C/\gamma T$, it cannot give rise to the non-mean-field behaviors observed in heat capacity and magnetic susceptibility above T_c.

Unusual crossover from Bardeen-Cooper-Schrieffer to Bose-Einstein-condensate superconductivity

In FeSe, while large superconducting fluctuations that well exceed the Gaussian fluctuations are observed, the C_e/T around T_c does not exhibit a significant deviation from the mean-field behavior. This suggests that tetragonal $FeSe_{1-x}S_x$ are closer to the BEC regime. However, with increasing S composition, the volume of the Fermi surface increases, as reported by quantum oscillation experiments[25], and Δ is reduced, according to STM measurements[33]. Then Δ/E_F is expected to become smaller with increasing S concentration, which is opposite to the tendency of approaching the BEC regime in the conventional BCS-BEC crossover. In fact, recent ARPES studies have reported BEC-like behavior in the tetragonal $FeSe_{1-x}S_x$[41], which is in good agreement with our thermodynamic studies. These behaviors are in contrast to the BEC-like dispersion observed for $Fe_{1+y}Se_xTe_{1-x}$[14] with increasing Δ/E_F, as expected in the context of conventional BCS–BEC crossovers. On the other hand, in our case of $FeSe_{1-x}S_x$, a structural phase transition from orthorhombic to tetragonal occurs as x increases. This leads to modification in the band structure and a significant change in the pairing interaction. This can be regarded as the main difference between the $Fe_{1+y}Se_xTe_{1-x}$ system and our $FeSe_{1-x}S_x$ system, leading to a change in the band structure and a significant change in pairing interactions. Another difference is that $FeSe_{1-x}S_x$ holds the compensation condition, where both electron and hole Fermi energies are comparably small, whereas the Fe non-stoichiometry in $Fe_{1+y}Se_xTe_{1-x}$ leads to the imbalance of Fermi energies of two carriers. This suggests that there is another important factor in the $FeSe_{1-x}S_x$ system which has not been duly taken into consideration.

A key factor that controls the BCS-BEC crossover in $FeSe_{1-x}S_x$ is the multiband character. As shown previously[16,21], in FeSe, the strong interband interaction between electron and hole pockets prevents the splitting of the T_{pair} and the T_c, determined by the superfluid stiffness. We note that this strong interband interaction is also an important ingredient in the orbital-selective scenario[29,42–44], and therefore we expect that even taking orbital selectivity into account, the main result, i.e., mean-field-like jump of the specific heat, will remain the same. At the same time, much less is known about the evolution of the ratio of the interband versus intraband interactions upon approaching x_c in $FeSe_{1-x}S_x$. Furthermore, recent experimental[45] and theoretical[46,47] works pointed out an interesting possibility of the substantial non-local nematic order on the d_{xy} orbital and/or inter-orbital-nematicity between d_{xy} and d_{yz} orbitals in FeSe. The most important consequence of this phenomenon would be an additional Lifshitz transition in $FeSe_{1-x}S_x$ upon S substitution, which occurs close to x_c. This, in turn, implies the appearance of the incipient band near x_c (see, for example, Fig. 6 in Rhodes et al. [46]). On general grounds, the presence of the incipient band would enhance the tendency towards the BCS-BEC crossover. In addition, given a nearly equal mixture of the s- and d-wave symmetry components of the superconducting gap in FeSe[48] to express such an anisotropic gap, it is natural to assume that they are competing in the tetragonal phase of $FeSe_{1-x}S_x$. In particular, the ratio of the pairing interactions in the d-wave and s-wave channels $|g^d_{ee}|/g^s_{eh}$ may, in addition to the incipient band, be another key parameter of the BCS-BEC crossover, as follows from our model calculations (Supplementary Note 4). The pair-formation temperature T_{pair} and condensation temperature T_c can be split more by increasing the ratio of intraband and interband interactions $|g^d_{ee}|/g^s_{eh}$ (Supplementary Note 4) without changing E_F. This quantitatively explains the appearance of strong coupling superconductivity for $x > x_c$ with no apparent enhancement of Δ/E_F. A remarkable and unexpected feature is the absence of pseudogap above T_c in the STS spectra, despite the presence of giant superconducting fluctuations in thermodynamic quantities. It should be noted that the relationship between the preformed pairs and the pseudogap formation is still elusive even in the ultra-cold atoms[2]. In addition, the onset temperature of the pseudogap may differ from that of fluctuations[31]. Moreover, it has been pointed out that the pseudogap phenomena in multiband systems are markedly altered from those in single-band systems. For instance, in multiband systems, the pseudogap formation is less prominent by the reduction of its onset temperature[49]. In a recent study, the BEC-like dispersion of the Bogoliubov quasiparticles has been reported in the tetragonal $FeSe_{1-x}S_x$ by using ARPES measurements[41]. Although the direct comparison of the ARPES data with the present thermodynamic results is not straightforward because ARPES measures only the portion of the hole Fermi pocket, it provides spectroscopic evidence of the BCS–BEC crossover. The ARPES measurements also report the presence of a distinct pseudogap in the hole pocket. However, we point out that this is not an apparent contradiction to the present STM results. It has been suggested that the DOS of electron pockets is much larger than that of hole pockets. As STM measures the DOS integrated over all bands, STM is insensitive to the pseudogap formation in the hole pocket. Therefore, the STM spectra, combined with the ARPES results, suggest that the pseudogap formation is also orbital-dependent.

It still, however, cannot fully explain the reduction of the gap magnitudes found experimentally, and further mechanisms may be needed, such as the influence of magnetic fluctuations, which would further reduce the superfluid stiffness[50], a Lifshitz transition near the orthorhombic to tetragonal transition[46], or nematic fluctuations. In $FeSe_{1-x}S_x$, the nematic fluctuations peaked at $q_{nem} \approx 0$ because it is ordered state breaks the rotational symmetry while preserving translational symmetry. Enhanced nematic fluctuations[22] play an important role in the normal state properties[23,51], particularly at $x \sim x_c$[23]. It has also been pointed out theoretically that nematic fluctuations strongly influence the superconductivity[52,53]. Therefore, it is tempting to consider that the nematic fluctuations and incipient bands in $FeSe_{1-x}S_x$ upon approaching a tetragonal phase can enhance the pairing interaction, leading the system to approach the BEC regime. Further theoretical and experimental studies are required to uncover whether the nematic fluctuations and multi-band nature affect the crossover physics.

Conclusion

Our thermodynamic studies have revealed a highly non-mean-field behavior of superconducting transition in $FeSe_{1-x}S_x$ when the nematic order of FeSe is completely suppressed by S substitution. This is consistent with the recent ARPES measurements, which report the BEC-like dispersion of the Bogoliubov quasiparticles in the tetragonal regime. Our findings demonstrate that $FeSe_{1-x}S_x$ offers a unique playground to study the superconducting properties in the BCS–BEC crossover regime of multiband systems.

Methods

Crystal growth and characterization. The single crystals of $FeSe_{1-x}S_x$ were grown by the chemical vapor transport technique as described in Böhmer et al. and Hosoi et al. [11,22]. The composition x is determined by energy-dispersive X-ray spectroscopy.

Heat capacity. The heat capacity of the crystals is measured using the long relaxation method[54,55] whose experimental setup is illustrated in the inset of Fig. 1a. A single bare chip of Cernox resistor is used as the thermometer, heater, and sample stage, which is suspended from the cold stage by silver-coated glass fibers in order that the bare chip has a weak thermal link to the cold stage and electrical connection for the sensor reading. The mass of the samples measured in this study is 81, 41, 171, 137, 179, 50, 107, 192, and 10 μg for $x = 0$, 0.05, 0.1, 0.13, 0.16, 0.18, 0.20#1, 0.20#2, and 0.21, respectively. The samples are mounted on the bare chip using Apiezon N grease. The heat capacity of the crystals is typically obtained by subtracting the heat capacity of the bare chip and grease from the raw data.

Magnetic torque. The torque measurements are performed using piezo-resistive micro-cantilevers[15]. The small single crystals with a typical size of 150 μm × 100 μm × 10 μm are mounted on the tip of microcantilevers with a small amount of Apiezon N grease. The magnetic field is applied inside the $ac(bc)$ plane by vector magnet, and the field-angle dependence of torque is obtained by rotating the whole cryostat within the $ac(bc)$ plane. Magnetic torque τ can be expressed as $\tau = \mu_0 V \boldsymbol{M} \times \boldsymbol{H}$, where μ_0 is vacuum permeability, V is sample volume, $\boldsymbol{M}$ is magnetization, and $\boldsymbol{H}$ is an external magnetic field. Here the $\boldsymbol{H}$ is rotated within the ac (bc) plane, and θ is the polar angle from the c-axis. In this configuration, the τ is expressed as $\tau_{2\theta}(T, H, \theta) = \frac{1}{2}\mu_0 H^2 V \Delta\chi \sin(\theta)$. Here $\Delta\chi = \chi_c - \chi_{ab}$ is anisotropy of magnetic susceptibility between the $ac(ab)$ plane and the c-axis.

Scanning tunneling microscopy/spectroscopy. The scanning tunneling microscopy/spectroscopy measurements have been performed with a commercial low-temperature STM system. Fresh and atomically flat surfaces are obtained by in situ cleavage at liquid nitrogen temperature in an ultra-high vacuum. All conductance spectra and topographic images are obtained by a PtIr tip. Conductance spectra are measured by a lock-in technique with a modulation frequency of 997 Hz and a modulation voltage of 200 μV. The backgrounds of raw conductance data are normalized by curves which are derived by 2nd-order polynomial fitting using outside superconducting gaps.

Theoretical calculation. The theoretical calculations were done within a simplified interacting two-band model in two dimensions, employed previously[21] with hole and electron pockets with small Fermi energies. We assume superconductivity is due to repulsive interactions. While the dominant interband interaction favors Cooper-pairing in the s-wave symmetry channel, the d-wave projected intraband interaction yields attraction in the d-wave channel. We obtained $T_{\rm pair}$ from the solution of the linearized mean-field gap equations, whereas T_c in each case is estimated from superfluid stiffness. Details of the calculations are given in the Supplementary Note 4.

Data availability

Most of the data in this study are available in the paper and supplementary information files. The other data, including raw data, can be provided upon request to the authors (Y.M.).

Code availability

The code of the analysis in this study is included in the supplementary information file.

Received: 5 April 2023; Accepted: 27 June 2023;
Published online: 19 July 2023

References

1. Sá de Melo, C. A. R. When fermions become bosons: pairing in ultracold gases. *Phys. Today* **61**, 45–51 (2008).
2. Randeria, M. & Taylor, E. Crossover from Bardeen-Cooper-Schrieffer to Bose-Einstein condensation and the unitary Fermi gas. *Annu. Rev. Condens. Matter Phys.* **5**, 209–232 (2014).
3. Strinati, G. C., Pieri, P., Röpke, G., Schuck, P. & Urban, M. The BCS-BEC crossover: from ultra-cold Fermi gases to nuclear systems. *Phys. Rep.* **738**, 1–76 (2018).
4. Chen, Q., Stajic, J., Tan, S. & Levin, K. BCS-BEC crossover: from high temperature superconductors to ultracold superfluids. *Phys. Rep.* **412**, 1–88 (2005).
5. Keimer, B., Kivelson, S. A., Norman, M. R., Uchida, S. & Zaanen, J. From quantum matter to high-temperature superconductivity in copper oxides. *Nature* **518**, 179–186 (2015).
6. Lubashevsky, Y. et al. Shallow pockets and very strong coupling superconductivity in $FeSe_xTe_{1-x}$. *Nat. Phys.* **8**, 309 (2012).
7. Kasahara, S. et al. Field-induced superconducting phase of FeSe in the BCS-BEC cross-over. *Proc. Natl. Acad. Sci. USA* **111**, 16309–16313 (2014).
8. Nakagawa, Y. et al. Gate-controlled BCS-BEC crossover in a two-dimensional superconductor. *Science* **372**, 190–195 (2021).
9. Suzuki, Y. et al. Mott-driven BEC-BCS crossover in a doped spin liquid candidate κ-$(BEDT\text{-}TTF)_4Hg_{2.89}Br_8$. *Phys. Rev. X* **12**, 011016 (2022).
10. Hsu, F.-C. et al. Superconductivity in the PbO-type structure α-FeSe. *Proc. Natl. Acad. Sci. USA* **105**, 14262–14264 (2008).
11. Böhmer, A. E. et al. Lack of coupling between superconductivity and orthorhombic distortion in stoichiometric single-crystalline FeSe. *Phys. Rev. B* **87**, 180505(R) (2013).
12. Shibauchi, T., Hanaguri, T. & Matsuda, Y. Exotic superconducting states in FeSe-based materials. *J. Phys. Soc. Jpn.* **89**, 102002 (2020).
13. Terashima, T. et al. Anomalous Fermi surface in FeSe seen by Shubnikov-de Haas oscillation measurements. *Phys. Rev. B* **90**, 144517 (2014).
14. Rinott, S. et al. Tuning across the BCS-BEC crossover in the multiband superconductor $Fe_{1+y}Se_xTe_{1-x}$: an angle-resolved photoemission study. *Sci. Adv.* **3**, e1602372 (2017).
15. Kasahara, S. et al. Giant superconducting fluctuations in the compensated semimetal FeSe at the BCS-BEC crossover. *Nat. Commun.* **7**, 12843 (2016).
16. Hanaguri, T. et al. Quantum vortex core and missing pseudogap in the multiband BCS-BEC crossover superconductor FeSe. *Phys. Rev. Lett.* **122**, 077001 (2019).
17. Coldea, A. I. & Watson, M. D. The key ingredients of the electronic structure of FeSe. *Annu. Rev. Condens. Matter Phys.* **9**, 125–146 (2018).
18. Vargunin, A. & Or¨d, T. Shrinking of the fluctuation region in a two-band superconductor. *Supercond. Sci. Technol.* **27**, 085006 (2014).
19. Sellin, K. A. H. & Babaev, E. First-order phase transition and tricritical point in multiband $U(1)$ London superconductors. *Phys. Rev. B* **93**, 054524 (2016).
20. Salasnich, L., Shanenko, A. A., Vagov, A., Albino Aguiar, J. & Perali, A. Screening of pair fluctuations in superconductors with coupled shallow and deep bands: a route to higher temperature superconductivity. *Phys. Rev. B* **100**, 064510 (2019).
21. Chubukov, A. V., Eremin, I. & Efremov, D. V. Superconductivity versus bound-state formation in a two-band superconductor with small Fermi energy: Applications to Fe pnictides/chalcogenides and doped $SrTiO_3$. *Phys. Rev. B* **93**, 174516 (2016).
22. Hosoi, S. et al. Nematic quantum critical point without magnetism in $FeSe_{1-x}S_x$ superconductors. *Proc. Natl. Acad. Sci. USA* **113**, 8139–8143 (2016).
23. Licciardello, S. et al. Electrical resistivity across a nematic quantum critical point. *Nature* **567**, 213–217 (2019).
24. Matsuura, K. et al. Maximizing T_c by tuning bematicity and magnetism in $FeSe_{1-x}S_x$ Superconductors. *Nat. Commun.* **8**, 1143 (2017).
25. Coldea, A. I. et al. Evolution of the low-temperature Fermi surface of superconducting $FeSe_{1-x}S_x$ across a nematic phase transition. *npj Quantum Mater.* **4**, 2 (2019).
26. Lin, J.-Y. et al. Coexistence of isotropic and extended s-wave order parameters in FeSe as revealed by low-temperature specific heat. *Phys. Rev. B* **84**, 220507(R) (2011).
27. Yang, H., Chen, G., Zhu, X., Xing, J. & Wen, H.-H. BCS-like critical fluctuations with limited overlap of Cooper pairs in FeSe. *Phys. Rev. B* **96**, 064501 (2017).
28. Hardy, F. et al. Calorimetric evidence of nodal gaps in the nematic superconductor FeSe. *Phys. Rev. B* **99**, 035157 (2019).
29. Sprau, P. O. et al. Discovery of orbital-selective Cooper pairing in FeSe. *Science* **357**, 75–80 (2017).
30. Pethick, C. J. & Smith, H. *Bose-Einstein Condensation in Dilute Gases*. (Cambridge University Press, 2008).
31. van Wyk, P., Tajima, H., Hanai, R. & Ohashi, Y. Specific heat and effects of pairing fluctuations in the BCS-BEC-crossover regime of an ultracold Fermi gas. *Phys. Rev. A* **93**, 013621 (2016).
32. Sato, Y. et al. Abrupt change of the superconducting gap structure at the nematic quantum critical point in $FeSe_{1-x}S_x$. *Proc. Natl. Acad. Sci. USA* **115**, 1227–1231 (2018).
33. Hanaguri, T. et al. Two distinct superconducting pairing states divided by the nematic end point in $FeSe_{1-x}S_x$. *Sci. Adv.* **4**, eaar6419 (2018).
34. Gati, E., Böhmer, A. E., Bud'ko, S. L. & Canfield, P. C. Bulk superconductivity and role of fluctuations in the iron-based superconductor FeSe at high pressures. *Phys. Rev. Lett.* **123**, 167002 (2019).
35. Pribulova, Z. et al. Upper and lower critical magnetic fields of superconducting $NdFeAsO_{1-x}F_x$ single crystals studied by Hall-probe magnetization and specific heat. *Phys. Rev. B* **79**, 020508(R) (2009).
36. Serafin, A. et al. Anisotropic fluctuations and quasiparticle excitations in $FeSe_{0.5}Te_{0.5}$. *Phys. Rev. B* **82**, 104514 (2010).
37. Welp, U. et al. Anisotropic phase diagram and superconducting fluctuations of single-crystalline $SmFeAsO_{0.85}F_{0.15}$. *Phys. Rev. B* **83**, 100513(R) (2011).
38. Inderhees, S. E. et al. Specific heat of single crystals of $YBa_2Cu_3O_{7-\delta}$: fluctuation effects in a bulk superconductor. *Phys. Rev. Lett.* **60**, 1178–1180 (1988).

39. Wiecki, P. et al. Persistent correlation between superconductivity and antiferromagnetic fluctuations near a nematic quantum critical point in $FeSe_{1-x}S_x$. *Phys. Rev. B* **98**, 020507(R) (2018).
40. Kuwayama, T. et al. NMR study under pressure on the iron-based superconductor $FeSe_{1-x}S_x$ ($x = 0.12$ and 0.23): relationship between nematicity and AF fluctuations. *Mod. Phys. Lett. B* **34**, 2040048 (2020).
41. Hashimoto, T. et al. Bose-Einstein condensation superconductivity induced by disappearance of the nematic state. *Sci. Adv.* **6**, eabb9052 (2020).
42. Yu, R., Zhu, J.-X. & Si, Q. Orbital selectivity enhanced by nematic order in FeSe. *Phys. Rev. Lett.* **121**, 227003 (2018).
43. Hu, H., Yu, R., Nica, E. M., Zhu, J.-X. & Si, Q. Orbital-selective superconductivity in the nematic phase of FeSe. *Phys. Rev. B* **98**, 220503(R) (2018).
44. Nica, E. M. & Si, Q. Multiorbital singlet pairing and $d + d$ superconductivity. *npj Quantum Mater.* **6**, 3 (2021).
45. Yi, M. et al. Nematic Energy Scale and the Missing Electron Pocket in FeSe. *Phys. Rev. X* **9**, 041049 (2019).
46. Rhodes, L. C., Böker, Jakob, Müller, M. A., Eschrig, M. & Eremin, I. M. Non-local d_{xy} nematicity and the missing electron pocket in FeSe. *npj Quantum Mater.* **6**, 45 (2021).
47. Steffensen, Daniel, Kreisel, Andreas, Hirschfeld, P. J. & Andersen, B. M. Interorbital nematicity and the origin of a single electron Fermi pocket in FeSe. *Phys. Rev. B* **103**, 054505 (2021).
48. Hashimoto, T. et al. Superconducting gap anisotropy sensitive to nematic domains in FeSe. *Nat. Commun.* **9**, 282 (2018).
49. Tajima, H., Yerin, Y., Pieri, P. & Perali, A. Mechanism of screening or enhancing the pseudogap throughout the two-band Bardeen-Cooper-Schrieffer to Bose-Einstein condensate crossover. *Phys. Rev. B* **102**, 220504 (2020).
50. Simard, O., Hébert, C.-D., Foley, A., Sénéchal, D. & Tremblay, A.-M. S. Superfluid stiffness in cuprates: effect of Mott transition and phase competition. *Phys. Rev. B* **100**, 094506 (2019).
51. Reiss, P. et al. Quenched nematic criticality and two superconducting domes in an iron-based superconductor. *Nat. Phys.* **16**, 89 (2020).
52. Maier, T. A. & Scalapino, D. J. Pairing interaction near a nematic quantum critical point of a three-band CuO_2 model. *Phys. Rev. B* **90**, 174510 (2014).
53. Lederer, S., Schattner, Y., Berg, E. & Kivelson, S. Superconductivity and non-Fermi liquid behavior near a nematic quantum critical point. *Proc. Natl. Acad. Sci. USA* **114**, 4905–4910 (2017).
54. Wang, Y., Revaz, B., Erb, A. & Junod, A. Direct observation and anisotropy of the contribution of gap nodes in the low-temperature specific heat of $YBa_2Cu_3O_7$. *Phys. Rev. B* **63**, 094508 (2001).
55. Taylor, O. J., Carrington, A. & Schlueter, J. A. Specific-heat measurements of the gap structure of the organic superconductors κ-$(ET)_2Cu[N(CN)_2]Br$ and κ-$(ET)_2Cu(NCS)_2$. *Phys. Rev. Lett.* **99**, 057001 (2007).

Acknowledgements

The authors thank A. Carrington, L. Malone, P. Walmsley, K. Ishida, K. Sugii, T. Taen, and T. Osada for experimental assistance. We also thank Y. Tada, H. Ikeda, K. Adachi, Y. Ohashi, and D. Inotani for their valuable discussion. This work has been supported by KAKENHI (Nos. JP23H01829, JP22H00105, JP22KK0036, JP21H04443, JP21KK0242, JP20H02600, JP20K21139, JP19H00649, JP18H05227, and JP18K13492), Grant-in-Aid for Scientific Research on Innovative Areas "Quantum Liquid Crystals" (No. JP19H05824) from JSPS, and CREST (No. JPMJCR19T5) from Japan Science and Technology (JST). The work of J.B. and I.E. is supported by the German Research Foundation within the bilateral NSFC-DFG Project ER 463/14-1. This work was partially carried out by the joint research in the Institute for Solid State Physics, the University of Tokyo.

Author contributions

Y. Mizukami and T.S. conceived and supervised the project. Y. Mizukami and O.T. developed the setup of heat capacity measurement and performed heat capacity measurements. M.H. performed STM/STS measurements. Y. Mizukami, K.M., D.S., and S.K. synthesized high-quality single crystals. J.B. and I.E. performed theoretical analysis. All authors discuss the results. Y. Mizukami prepared the paper with inputs from I.E., Y. Matsuda, and T.S.

Competing interests

The authors declare no competing interests.

Additional information

Supplementary information The online version contains supplementary material available at https://doi.org/10.1038/s42005-023-01289-8.

Correspondence and requests for materials should be addressed to Yuta Mizukami.

Peer review information *Communications Physics* thanks the anonymous reviewers for their contribution to the peer review of this work.

Reprints and permission information is available at http://www.nature.com/reprints

Publisher's note Springer Nature remains neutral with regard to jurisdictional claims in published maps and institutional affiliations.